Biophysical Journal
Article

Biophysical Society

Changes in Cholesterol Level Alter Integrin Sequestration in Raft-Mimicking Lipid Mixtures

Yifan Ge,[1] Jiayun Gao,[1] Rainer Jordan,[3] and Christoph A. Naumann[1,2,*]
[1]Department of Chemistry and Chemical Biology and [2]Integrated Nanosystems Development Institute, Indiana University-Purdue University Indianapolis, Indianapolis, Indiana; and [3]Makromolekulare Chemie, TU Dresden, Dresden, Germany

ABSTRACT The influence of cholesterol (CHOL) level on integrin sequestration in raft-mimicking lipid mixtures forming coexisting liquid-ordered (l_o) and liquid-disordered (l_d) lipid domains is investigated using complementary, single-molecule-sensitive, confocal detection methods. Systematic analysis of membrane protein distribution in such a model membrane environment demonstrates that variation of CHOL level has a profound influence on l_o-l_d sequestration of integrins, thereby exhibiting overall l_d preference in the absence of ligands and l_o affinity upon vitronectin addition. Accompanying photon-counting histogram analysis of integrins in the different model membrane mixtures shows that the observed changes of integrin sequestration in response to variations of membrane CHOL level are not associated with altering integrin oligomerization states. Instead, our experiments suggest that the strong CHOL dependence of integrin sequestration can be attributed to CHOL-mediated changes of lipid packing and bilayer thickness in coexisting l_o and l_d domains, highlighting the significance of a biophysical mechanism of CHOL-mediated regulation of integrin sequestration. We envision that this model membrane study may help clarify the influence of CHOL in integrin functionality in plasma membranes, thus providing further insight into the role of lipid heterogeneities in membrane protein distribution and function in a cellular membrane environment.

INTRODUCTION

Cholesterol (CHOL), the main sterol lipid in the plasma membrane, plays an important, multifaceted role in the regulation of membrane protein function. Its functional significance is illustrated by the observation that abnormal levels of membrane CHOL level are associated with several diseases, such as Alzheimer's disease and diabetes (1). Membrane CHOL may influence properties of membrane proteins either by serving as ligand or by altering biophysical properties of the membrane environment (2,3). Prominent examples of CHOL as membrane protein ligand include the CHOL-mediated regulation of acetylcholine and GPCR receptor functionality (4–6). CHOL impacts biophysical properties of membranes by enhancing lipid packing density and bilayer thickness. For example, lipid diffusion experiments in different types of model membranes have established that addition of CHOL to a phospholipid bilayer leads to a drop of lipid diffusivity, illustrating the impact of CHOL on lipid packing (7,8). Neutron diffraction experiments have established that incorporation of 29 mol% CHOL into a 1,2-dioleoyl-*sn*-glycero-3-phosphocholine (DOPC) bilayer is associated with an increase in bilayer thickness of 2.8 Å, which corresponds to 5.6% of the DOPC bilayer thickness (9). CHOL-mediated changes in bilayer thickness are considered to be significant as they alter hydrophobic matching conditions between the hydrophobic membrane thickness and the thickness of the transmembrane region of embedded membrane proteins. Most prominently, such hydrophobic matching arguments have been made to explain the sorting of transmembrane proteins along the secretory pathway (10). CHOL incorporation into a phospholipid bilayer not only influences bilayer thickness and lipid packing, but also leads to increased membrane bending stiffness. In the latter case, membrane protein distribution may be affected by constraining the adaptability of the bilayer in the case of hydrophobic mismatch (11). Another important property of membrane CHOL represents its particular affinity for sphingolipids (SL), leading to the formation of lipid rafts (12). These CHOL-enriched membrane domains are considered to be crucial regulators of membrane protein distribution and function, thereby influencing multiple processes, including membrane trafficking and membrane signaling (13). Control of protein sorting through lipid packing density differences between coexisting CHOL-enriched and

Submitted November 1, 2017, and accepted for publication November 6, 2017.

*Correspondence: canauman@iupui.edu

Editor: Kalina Hristova.
https://doi.org/10.1016/j.bpj.2017.11.005

CHOL-deficient domains is supported by previous energetic calculations and by simulations on bilayer-spanning peptides (14,15). Other studies have emphasized the significance of hydrophobic matching in explaining the sorting of membrane proteins in a heterogeneous membrane environment (16).

The importance of CHOL in membrane protein functionality is exemplified by a strong link between membrane CHOL level and integrin signaling and adhesion. For example, CHOL was reported to play a crucial role in the assembly of signaling complexes, which involve $\alpha_v\beta_3$-integrins, G-proteins, and CD47 (17). The significance of CHOL in integrin-mediated cell adhesion formation was demonstrated by the observation that integrin assembly at cellular focal adhesions is closely related to a certain membrane CHOL level (18). Consistent with this observation, Gaus et al. (19) previously reported that the lipid environment at focal adhesion sites is highly enriched in CHOL, whereas cell detachment causes internalization of lipid rafts and decreased lipid order (i.e., membrane CHOL level) in the plasma membrane. The above findings suggest a close interplay between integrin adhesion/signaling and recruitment of these membrane proteins to lipid rafts. Indeed, it previously has been reported that integrins LFA-1 and $\alpha_4\beta_1$ are recruited to raft domains upon activation with extracellular matrix ligands (20). Furthermore, recent coarse-grained molecular dynamics simulations revealed a CHOL annulus around integrin-talin complexes (21). However, the role of membrane CHOL level in the biophysical regulation of integrin sequestration and recruitment processes during raft-mediated integrin adhesion and signaling remains poorly understood. This lack of knowledge can be attributed, at least in part, to the challenging characterization of the typically small and transient raft domains in the plasma membrane (22,23).

To overcome experimental challenges associated with cellular studies, protein sorting processes have also been explored in model membrane systems, which enable the characterization of membrane proteins in the presence of coexisting, micron size, liquid-ordered (l_o) and liquid-disordered (l_d) domains (24,25). Our group also built on a model membrane strategy and previously determined the sequestration and oligomerization state of integrins and urokinase plasminogen activator receptors (uPARs) in raft-mimicking lipid mixtures using complementary confocal fluorescence detection techniques of single-molecule sensitivity, which include two-dimensional confocal imaging, fluorescence correlation spectroscopy (FCS), and the photon-counting histogram (PCH) method. By applying this methodology, we confirmed findings from cellular studies (26,27) that uPAR dimerization and sequestration in raft-mimicking model lipid mixtures can be controlled by exposure to distinct native ligands, but not through variation of membrane CHOL level (28). Another set of experiments demonstrated that native ligands and bilayer asymmetry alter the sequestration of integrins in raft-mimicking lipid mixtures (29,30). Although our data suggest that native ligands alter integrin sequestration through ligand-induced allosteric changes of integrin receptors without altering integrin oligomerization state, the observed bilayer asymmetry dependence illustrates the potential significance of differences in lipid packing and bilayer thickness between l_o and l_d domains in the receptor sequestration process. Here, we demonstrate that systematic changes in membrane CHOL content have a notable impact on the sequestration of $\alpha_v\beta_3$-integrin in coexisting l_o and l_d domains, thereby displaying qualitatively different sequestration behavior in the absence and presence of its native ligand vitronectin (VN). Notably, the accompanying domain-specific analysis of lipid diffusivity indicates that CHOL may act as a regulator of integrin distribution by distinctly altering bilayer thickness and lipid packing density in l_o and l_d domains. These results are intriguing because they support the potential importance of biophysical mechanisms in the observed interplay between CHOL level and integrin distribution in cellular membranes.

MATERIALS AND METHODS

Materials

The phospholipids DOPC, 1,2-dipalmitoyl-*sn*-glycero-3-phosphocholine (DPPC), and CHOL were purchased from Avanti Polar Lipids (Alabaster, AL). The lipopolymer 1,2-dioctadecyl-*sn*-glycero-3-N-poly(2-methyl-2-oxazoline)$_{50}$ was synthesized as reported previously (31). The dye-labeled phospholipids N-(7-nitrobenz-2-oxa-1,3-diazol-4-yl)-1,2-dihexadec-anoyl-*sn*-glycero-3-phosphoethanolamine, triethylammonium salt (NBD-DHPE) and N-(6-tetramethylrhodamine-thiocarbamoyl)-1, 2-dihexadecanayl-*sn*-glycero-3-phosphoethanolamine, triethylammonium salt (TRITC-DHPE) were obtained from Invitrogen (Carlsbad, CA). Purified human $\alpha_v\beta_3$-integrin, purified VN, and anti-β_3-integrin monoclonal antibody (MAb) (clone HMb3-1) were purchased from EMD Millipore (Billerica, MA). Human uPAR and anti-DDK antibody were both obtained from Origene Technologies (Rockville, MD). Dye-labeling of MAb was accomplished through interaction between free-amine groups of IgG and carboxylic acid groups of Alexa 555 dyes using Alexa 555 microscale protein labeling kits (ThermoFisher, Waltham, MA), following standard protocols provided by the vendor. FCS autocorrelation analysis of dye-labeled antibodies in solution confirmed that the labeling procedure resulted in 2–2.5 dye molecules per MAb. The fluorescence standard rodamine-6-G was purchased from Sigma-Aldrich (St. Louis, MO). The surfactant *n*-octyl-β-D-glucopyranoside (OG) was obtained from Fisher BioReagents (Fairlawn, NJ). High performance liquid chromatography grade chloroform was acquired from Fisher Scientific (Pittsburgh, PA).

Construction of polymer-tethered lipid bilayer

The distribution and oligomerization state of membrane proteins in raft-mimicking lipid mixtures was analyzed using a polymer-tethered lipid bilayer. This planar membrane system was chosen because the lift-up of the lipid bilayer by the underlying polymer cushion makes it well suited for the characterization of transmembrane proteins using single-molecule-sensitive optical detection techniques. Furthermore, unlike coexisting l_o and l_d domains in a solid-supported lipid bilayer, those in a polymer-tethered lipid bilayer can span the whole bilayer, a beneficial property in the

described protein sequestration studies (32). Polymer-tethered lipid bilayers were built using the Langmuir-Blodgett (LB)/Langmuir-Schaefer (LS) method to achieve an asymmetric bilayer composition (i.e., bottom leaflet of bilayer contains lipids with 5 mol% lipopolymers; top leaflet is comprised of lipids). This LB/LS fabrication method has been described elsewhere (32,33). In short, a lipid monolayer at the air-water interface (subphase: Milli-Q water [pH 5.5], 18 MΩ-cm resistivity) was compressed to a film pressure of 30 mN/m and, after an incubation time, was transferred to a precleaned glass coverslip using the dipper of the LB trough (Labcon, Darlington, UK). This process was followed by the LS process, in which the LB-functionalized glass substrate is gently pushed through another lipid monolayer at the air-water interface. The resulting LB/LS bilayer was transferred to a petri dish filled with Milli-Q water, which was later replaced with phosphate-buffered saline (PBS) to allow the reconstitution of membrane proteins. To investigate the influence of CHOL levels on integrin sequestration, ternary DOPC/DPPC/CHOL mixed bilayers were constructed, which contained equimolar concentrations of DOPC and DPPC and varying concentrations of CHOL of 28, 30, 33, 35, and 37 mol%. The LB monolayer also contained 5 mol% of the lipopolymer 1,2-dioctadecyl-*sn*-glycero-3-N-poly(2-methyl-2-oxazoline)$_{50}$ to lift the bilayer from the glass substrate. To visualize coexisting l_o-l_d domains using fluorescence detection techniques and to assure their bilayer-spanning nature in regions of protein analysis, both LB and LS monolayers were labeled with 0.2 mol% NBD-DHPE. The formation of coexisting l_o-l_d domains in NBD-DHPE-containing lipid mixtures characteristic for the bottom and top leaflets of the bilayer was also confirmed in LB monolayers of those mixtures before bilayer assembly.

Reconstitution and labeling of membrane proteins

The reconstitution of membrane proteins into the polymer-tethered lipid bilayer was pursued using a modified Rigaud method following established procedures described before (29,34). In short, 1.3×10^{-11} mol $\alpha_V\beta_3$-integrin or uPAR were added to the preassembled polymer-tethered lipid bilayer with the assistance of 250 μM OG, and incubated for 2.5 h. The added amount of OG corresponds to just 0.2% of its bilayer-dissolving concentration, ensuring the bilayer stability during the protein reconstitution process. A single layer of SM-2 Bio-Beads (Bio-Rad, Hercules, CA) was added and incubated for less than 10 min, followed by extensive rinsing with PBS, thus removing OG from the bilayer sample. To fluorescently label membrane proteins in the bilayer, Alexa 555-labeled MAb (anti-β_3-integrin MAb [$\alpha_V\beta_3$] or anti-DDK MAb [uPAR]) were allowed to bind to reconstituted membrane proteins during an incubation time of 2 h. Here, MAb were added in a 1.5- or 10-fold (control) molar excess (relative to membrane proteins) to suppress antibody-mediated cross-linking of membrane proteins in the bilayer. Next, unbound Alexa 555 MAb were washed off using PBS to enable characterization of fluorescently tagged membrane proteins in the bilayer samples. The antibody labeling approach was chosen because, unlike a direct protein labeling method, it allows the selective tagging of correctly oriented and properly folded membrane proteins, thus improving the accuracy and reliability of their characterization in the bilayer samples using quantitative fluorescence intensity analysis methods. The MAb labeling of integrins is widely established (35) and benefits from the large extracellular epitope of these receptors (36). Integrin sequestration/oligomerization experiments were also conducted in the presence of VN, a native ligand of $\alpha_V\beta_3$. In this case, an equimolar amount of VN (relative to $\alpha_V\beta_3$) was added to the integrin-containing bilayer sample and incubated overnight. Before imaging analysis, the sample was rinsed with PBS to remove unbound VN. Separate experiments on integrins in the absence and presence of VN were included to explore the role of CHOL level in integrin sequestration using two different integrin conformations representing inactive ($\alpha_v\beta_3$) and ligand-activated ($\alpha_v\beta_3$ and VN) states of this receptor (29).

Microscopy techniques

A commercial microscopy system (Carl Zeiss, Jena, Germany) was employed that allows the analysis of bilayer samples using standard epifluorescence (EPI) microscopy and confocal fluorescence detection. The system is equipped with an Axiovert 200M inverted microscope with EPI illumination (Carl Zeiss, Oberkochen, Germany), a Zeiss C-Apochromat objective (water immersion, 40$\times$ NA = 1. 2), a Zeiss AxioCam MRm monochrome digital camera, an LSM510 laser excitation module, and a ConfoCor 2 FCS module. The ConfoCor 2 module contains two highly sensitive avalanche photo diode detectors, enabling quantitative fluorescence intensity analysis experiments on fluorescently tagged membrane proteins with single-molecule sensitivity. The microscope system is equipped with a X-Y-Z scanning stage, which can be employed to conduct two-dimensional confocal scans (CS-XY scans) in planar model membranes. The spatial resolution of such scans is limited by the step size of the scanner of 0.5 μm. Importantly, this confocal methodology is well suited for the domain-specific readout of fluorescence intensity data because the size of the confocal spot of $\sim$0.5 μm is small in comparison to the typical size of l_o/l_d domains in lipid mixtures employed. EPI experiments, operated in EPI illumination using the Zeiss AxioCam MRm monochrome digital camera in combination with Axiovision 4.8 software, were conducted to confirm large-scale l_o and l_d phase separations in select lipid mixtures of varying membrane CHOL level. In contrast to confocal fluorescence intensity data acquisition, EPI micrographs were acquired using automatic contrast enhancement, enabling better visualization of domains under conditions of low contrast. To determine the distribution and oligomerization of integrins in the bilayer, confocal fluorescence intensity analysis experiments were pursued using laser excitation and ConfoCor 2 detection. In this case, Alexa 555 MAb-labeled integrins were analyzed using a 1.8 mW HeNe laser (543 nm) in combination with a 560–605 nm emission filter (red channel), whereas parallel analysis of dye-labeled lipids (NBD-DHPE) was achieved using a 30 mW Argon laser (514 nm) with a 500–530 nm emission filter (green channel). Protein sequestration was explored by conducting CS-XY scans of planar model membrane samples through the green (lipid) and red (protein) detection channels, thereby utilizing the piezo-scanning stage of the microscope system (scan size: 12 $\times$ 12 μm; scan step: 0.5 μm). Here the green (lipid) channel data were utilized to select l_o and l_d regions for protein sequestration analysis using the red (protein) channel. In addition, the confocal spot was kept at fixed l_o and l_d bilayer positions and the photon counts in the red channel were collected over a time period of 50 s, enabling domain-specific PCH analysis of laterally mobile membrane proteins in the bilayer. The ConfoCor 2 system was also employed to obtain domain-specific information about lipid (TRITC-DHPE) diffusivity in coexisting l_o and l_d domains using FCS autocorrelation analysis. In this assay, both leaflets of the protein-free bilayer were labeled with 0.2 mol% NBD-DHPE to visualize lipid domains (green channel) and 0.001 mol% of the lipid diffusion probe TRITC-DHPE (red channel). By adapting a previously reported experimental procedure, FCS diffusion times were expressed in terms of diffusion coefficients using a TRITC-DHPE standard, for which a diffusion coefficient was available form independent, wide-field, single-molecule fluorescence microscopy experiments (30). All imaging experiments were conducted in divalent, cation-free PBS at a temperature of 25°C.

Data analysis

The quantitative analysis of membrane protein sequestration and dimerization in model lipid mixtures of different CHOL content follows established procedures described previously (29). To analyze the sequestration of Alexa 555 MAb-tagged membrane proteins ($\alpha_V\beta_3$ or uPAR) in raft-mimicking model lipid mixtures, CS-XY raw data were first corrected for NBD-DHPE bleed through in the Alexa 555 channel, which is $\sim$6% of the total background, and nonspecific adsorption of Alexa 555 MAbs on the lipid bilayer. The latter background contribution was obtained in separate control CS-XY scan experiments, in which comparable amounts of Alexa

555-tagged MAbs were added to membrane protein-free bilayers of corresponding lipid composition. The overall signal/background (through the Alexa 555 channel) for Alexa 555 MAb-tagged membrane proteins in the bilayer containing NBD-DHPE was determined to be ~4:1. Next, the receptor distribution in the raft-mimicking lipid mixtures was quantified in terms of the parameter E_{raft}, which is defined as

$$E_{raft} = \frac{I_{lo} - I_{ld}}{I_{lo} + I_{ld}}, \quad (1)$$

with I_{lo} and I_{ld} describing the background-corrected average signal intensities of the fluorescently tagged membrane proteins in the l_o and l_d phases, respectively. According to Eq. 1, positive values of E_{raft} indicate accumulation of probe molecules in the l_o phase, negative E_{raft} values suggest higher affinity for the l_d phase, and $E_{raft} = 0$ is representative of a lacking lipid phase preference. To assure reproducibility, E_{raft} values were acquired from at least 15 different bilayer spots ($12 \times 12\ \mu m^2$) of three different bilayer samples. From the E_{raft} data at 33 and 37 mol% CHOL, we also identified the fraction of membrane proteins, $X_{migrate}$, which alter their phase preference in response to such a change in membrane CHOL. To determine $X_{migrate}$, one considers that the number of molecules, N_T, which alter their phase preference, is associated with a characteristic fluorescence intensity, I_T. Then E_{raft} at 37 mol% CHOL can be expressed as

$$E_{raft}(37\ \text{mol\% CHOL}) = \frac{\left[I_{lo}^{37} - I_{ld}^{37}\right]}{I_{lo}^{37} + I_{ld}^{37}} = \frac{\left[\left(I_{lo}^{33} - I_T\right) - \left(I_{ld}^{33} + I_T\right)\right]}{I_{lo}^{33} + I_{ld}^{33}}. \quad (2)$$

The mole fraction of molecules, $X_{migrate}$, which translocate from l_o to l_d between 33 and 37 mol% CHOL, can now be written as

$$X_{migrate} = \frac{1}{2}\frac{\left[I_{lo}^{33} - I_{ld}^{33}\right] - \left[\left(I_{lo}^{33} - I_T\right) - \left(I_{ld}^{33} + I_T\right)\right]}{I_{lo}^{33} + I_{ld}^{33}} = \frac{I_T}{I_{lo}^{33} + I_{ld}^{33}}. \quad (3)$$

The factor 1/2 was introduced to correct for double counting. Eq. 3 can also be expressed as

$$X_{migrate} = \left|\frac{E_{raft(33\ \text{mol\% CHOL})} - E_{raft(37\ \text{mol\% CHOL})}}{2}\right|. \quad (4)$$

A comparable type of Eq. 4, which determines the mole fraction of translocated membrane proteins between l_o and l_d in response to ligand binding, was introduced previously (29).

Raw data of photon counts at fixed bilayer positions were also collected over a time period of 50 s and analyzed using the PCH method, thereby adapting methods reported previously (29). Particle brightness and sample-specific background were first determined in separate control experiments to enable the accurate analysis of dimerization level of Alexa 555 MAb-labeled $\alpha_V\beta_3$ in the bilayer samples. In one control assay, FCS autocorrelation analysis experiments were pursued to identify the average brightness of individual Alexa 555 MAb in solution. The brightness of fluorescent probes in solution and bound to a supported lipid bilayer was previously established to be identical within 5%, on our imaging setup (29). In another control assay, Alexa 555-labeled MAb were added, incubated, and rinsed off on corresponding integrin-free lipid bilayers, providing information about sample-specific background. With the sample-specific brightness and background values being determined, experimentally determined PCH curves were modeled using a PCH algorithm to provide information about average brightness and number of Alexa 555 MAb-labeled membrane protein monomers (ε, N_{avg}) and dimers ($\varepsilon_{dimer} = 2\varepsilon$, $N_{avgdimer}$) in the different planar model lipid mixtures. The level of receptor dimerization can be quantified in terms of the mole fraction of dimers, X_{dimer}. The PCH algorithm was created by assuming a Gaussian point spread function. To account for non-Gaussian shape contributions to the point spread function, noticeable at low concentrations, the primary species was convoluted with a second species of low brightness and high number. The variance and χ^2 of fitting data can be expressed by

$$\chi^2 = \frac{\sum_{kmin}^{kmax} \frac{(p(k) - \text{PCH}(k))^2}{p(k)(1-p(k))}}{k_{max} - k_{min} - d}, \quad (5)$$

where d is the number of fitting parameters, $p(k)$ the experimentally determined probability of observing k photon counts, PCH(k) is the PCH algorithm-generated probability of observing k photon counts, and $p(k)(1 - p(k))$ is a specialized variance to account for substantial variations of values at different k. For each lipid composition, photon counts for PCH analysis were acquired from at least 50 different spots of l_o and l_d regions. Standard deviations of the resulting PCH data sets are illustrated as error bars in the presented X_{dimer} data. The PCH method was previously tested using monomeric fluorescent probes, such as organic dyes and CdSe/ZnS quantum dots, in solution and bound to lipids in a planar lipid bilayer (29). The surface functionalization of such quantum dots and their specific linkage to lipid bilayers has been described elsewhere (37). In addition, the PCH method was validated by determining that binding of certain ligands (VN and uPAR) leads to substantial changes in the degree of dimerization of the glycosylphosphatidylinositol (GPI)-anchored uPAR, in excellent agreement with cellular studies (26,28). The statistical significance of all presented data (lateral diffusion coefficients, X_{dimer}, E_{raft}) was verified by comparing independent data sets using T-tests and/or analysis of variance tests.

RESULTS AND DISCUSSION

Impact of CHOL on lipid mixing behavior and l_o-l_d lipid diffusivities

Before experiments on integrin-containing bilayers, we first analyzed the lipid mixing behavior of different DOPC/DPPC/CHOL mixtures in a polymer-tethered lipid bilayer using EPI. Fig. 1 illustrates representative EPI micrographs of such ternary lipid mixtures containing 0.2 mol% NBD-DHPE. Here the lipid mixtures are comprised of equimolar concentrations of DOPC and DPPC and varying concentrations of CHOL at 25, 28, 33, 35, 37, and 40 mol% CHOL. Fig. 1 reveals the formation of optically visible phase separations in lipid mixtures with CHOL molar concentrations ranging from 25 to 37 mol%. In contrast, the bilayer sample with 40 mol% CHOL is free of any optically visible domains, indicating a phase boundary between 37 and 40 mol% CHOL similar to comparable lipid mixtures in vesicular systems (38). Previously, we reported that NBD-DHPE shows a l_o phase preference in a polymer-tethered lipid bilayer containing raft-mimicking lipid mixtures (note: NBD-DHPE is not always an l_o marker in model membranes) (29). This finding suggests that the bright phase in micrographs with coexisting lipid domains in Fig. 1 display bilayer regions enriched in CHOL and DPPC, whereas the coexisting dark phase shows corresponding bilayer areas enriched in DOPC.

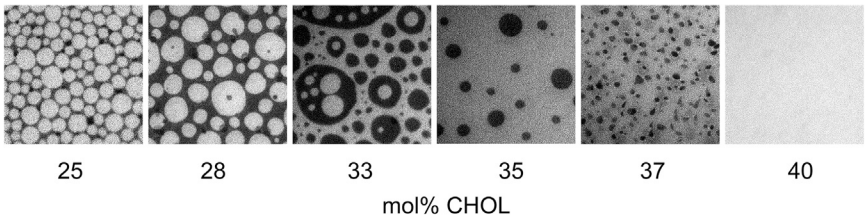

FIGURE 1 Representative EPI micrographs of NBD-DHPE distribution in a polymer-tethered lipid bilayer that contains equimolar concentrations of DOPC and DPPC and varying CHOL molar concentration of 25, 28, 33, 35, 37, and 40 mol%.

Next, we determined the impact of CHOL level on TRITC-DHPE lateral mobility in coexisting lipid domains using FCS autocorrelation analysis, thereby employing the same phase separating bilayer compositions as described in Fig. 1. The resulting TRITC-DHPE lateral diffusion data from these FCS experiments are summarized in Fig. 2 *A*. They demonstrate that both lipid phases are characterized by distinct TRITC-DHPE diffusivities, consistent with the concept of coexisting l_o and l_d phases (39). The analysis of TRITC-DHPE diffusion coefficients in Fig. 2 *A* also confirms that increases in CHOL molar concentration in the bilayer cause the domain-specific elevation of CHOL content (decreased TRITC-DHPE diffusion) in both lipid phases. Moreover, Fig. 2 *A* shows that differences in TRITC-DHPE diffusivity between l_o and l_d are most pronounced at 28 and 33 mol% CHOL, intermediate at 35 mol% CHOL, and rather small at 25 and 37 mol% CHOL, respectively. The well-established effect of CHOL on phospholipid diffusivity was confirmed in control experiments of FCS autocorrelation analysis of TRITC-DHPE in DOPC and binary DOPC-CHOL mixtures of 15 and 30 mol% CHOL, which provided lipid diffusion values of $D^{\mathrm{TRITC-DHPE}}_{0\mathrm{mol\%CHOL}} = 1.63 \pm 0.26\ \mu\mathrm{m}^2/\mathrm{s}$, $D^{\mathrm{TRITC-DHPE}}_{15\ \mathrm{mol\%CHOL}} = 1.31 \pm 0.15\ \mu\mathrm{m}^2/\mathrm{s}$, and $D^{\mathrm{TRITC-DHPE}}_{30\ \mathrm{mol\%CHOL}} = 1.20 \pm 0.06\ \mu\mathrm{m}^2/\mathrm{s}$.

Comparison of lipid diffusivity in CHOL-containing lipid mixtures in a planar polymer-tethered lipid bilayer, as presented in this study, with corresponding data in giant unilamellar vesicles (GUVs) (8) reveals interesting similarities and some differences. In both model membrane systems, an increase in membrane CHOL between 0 and 30 mol% in a binary DOPC-CHOL lipid mixture leads to a roughly 25% reduction in lipid diffusivity, suggesting a similar effect of CHOL on fluidity. In the GUV system, different l_o-l_d diffusivities are observed in ternary DOPC/DPPC/CHOL mixtures between 12 and 32 mol% CHOL. Similarly, the domain-specific diffusion data in Fig. 2 *A* suggest that there is a certain region of CHOL compositions, which is characterized by different l_o-l_d diffusivities. However, the boundaries of this region are shifted, ranging from ~25 to 37 mol% CHOL. Both types of membrane systems also vary in terms of the maximum ratio of diffusivities in l_d and l_o domains, which is $D_{ld}/D_{lo}(\mathrm{max}) \sim 12$ in the GUV system (8) and $D_{ld}/D_{lo}(\mathrm{max}) \sim 1.4$ in the polymer-tethered lipid bilayer system (Fig. 2 *A*). Furthermore, our fluorescence experiments in polymer-tethered lipid bilayer systems did not provide experimental evidence for gel domains in ternary DOPC/DPPC/CHOL mixtures of lower CHOL content, as observed in vesicular model membranes of corresponding lipid composition (40). Together, these results suggest that the perturbing effect of polymer-tethered lipids may influence l_o/l_d packing and lipid mixing behavior in the polymer-tethered lipid bilayer.

The lipid diffusion data in Fig. 2 *A* can be considered as a measure of domain-specific lipid packing because 1) raft-mimicking lipid mixtures (e.g., DOPC/DPPC/CHOL) are characterized by the coexistence of CHOL-enriched (l_o) and CHOL-deficient (l_d) lipid domains; 2) increasing CHOL concentration leads to reduced lipid lateral mobility; and 3) lipid diffusion in a polymer-tethered membrane is well described by a free-area model (7,8,38,41). A hallmark of such a free-area model is that probe diffusion depends on area per lipid, a measure of lipid packing, but not membrane thickness. Consistent with our experimental findings,

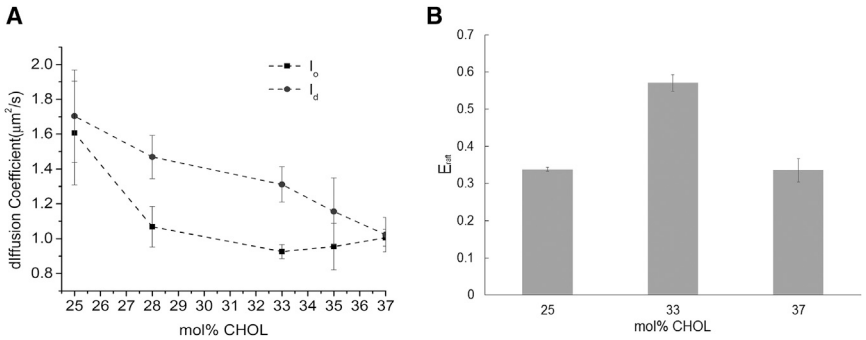

FIGURE 2 Analysis of domain-specific TRITC-DHPE diffusivity (*A*) and E_{raft} data of NBD-DHPE distribution (*B*) suggest that variation in membrane CHOL between 25 and 37 mol% CHOL alters lipid packing differences between l_o and l_d domains of a polymer-tethered lipid bilayer containing DOPC/DPPC/CHOL mixtures (1:1 DOPC/DPPC molar ratio); $p < 0.005$. Error bars represent standard deviation of data sets from 15 different bilayer regions (out of three samples).

differences in l_o-l_d lipid packing have previously been shown to influence the partitioning of another lipid probe, GM_1 (42).

The influence of CHOL on l_o-l_d lipid packing differences is also supported by the corresponding sequestration data of dye-labeled lipids (NBD-DHPE) in polymer-tethered lipid bilayers containing equimolar amounts of DOPC and DPPC and varying CHOL concentrations of 25, 33, and 37 mol% CHOL (Fig. 2 *B*). In this case, we conducted two-dimensional confocal scans (CS-XY scans) of the bilayer samples with coexisting lipid domains (representative CS-XY scans of NBD-DHPE distribution are shown in Fig. 3, *A–C*) and determined the E_{raft} values of NBD-DHPE distribution. Notably, there is a good qualitative correlation between the l_o-l_d diffusion difference (Fig. 2 *A*) and the corresponding l_o-l_d sequestration of dye-labeled lipids (Fig. 2 *B*). At 33 mol% CHOL, both E_{raft} data of NBD-DHPE and l_o-l_d diffusion difference of TRITC-DHPE are largest, indicating the most pronounced lipid packing difference between l_o and l_d. In contrast, E_{raft} values of NBD-DHPE and l_o-l_d diffusion difference of TRITC-DHPE associated with 25 and 37 mol% CHOL are significantly reduced, suggesting similar packing conditions between both types of domains without reaching the phase boundary of the coexistence region yet (as shown by visible domains in Fig. 1).

CHOL level influences sequestration of $\alpha_V\beta_3$ and $\alpha_V\beta_3$ with VN

By adapting procedures described before (29,30), we next conducted two-dimensional confocal scans (CS-XY scans) of NBD-DHPE and $\alpha_V\beta_3$-integrin distributions in a polymer-tethered lipid bilayer comprised of ternary DOPC/DPPC/CHOL mixtures containing equimolar amounts of DOPC and DPPC and varying CHOL concentrations of 25, 28, 33, 35, and 37 mol%. Here integrins were labeled with Alexa 555 antibody to allow dual-color fluorescence imaging and analysis in the presence of NBD-DHPE enabling visualization of lipid domains. Initially, the integrin distribution in the different bilayer mixtures was determined in the absence of ligands [VN(−)]. Fig. 3, *A–F* shows representative CS-XY scans (raw data) of bilayer samples from these experiments through the NBD (Fig. 3, *A–C*) and Alexa 555 channels (Fig. 3, *D–F*) for 25 mol% (Fig. 3, *A* and *D*), 33 mol% (Fig. 3, *B* and *E*), and 37 mol % CHOL (Fig. 3, *C* and *F*). Analysis of the NBD channel CS-XY scans confirms the presence of large-scale, lipid-lipid phase separations for all three samples consistent with the EPI data of lipid mixing behavior presented in Fig. 1. Notably, comparison of the NBD-channel CS-XY scans with corresponding Alexa 555 channel data (Fig. 3, *D–F*) shows that changes in CHOL content have a significant effect on the distribution of integrins in the DOPC/DPPC/CHOL mixed bilayer system. Although the CS-XY scans of lipid mixtures with 25 (Fig. 3 *D*) and 37 mol% CHOL (Fig. 3 *F*) do not display any substantial sequestration of integrins, that of 33 mol% CHOL does. In the latter case, comparison of NBD (Fig. 3 *B*) and Alexa 555 channel data (Fig. 3 *E*) demonstrates that the pattern of integrin sequestration is consistent with the l_o-l_d phase boundaries for this bilayer. Here Alexa 555 antibody-labeled $\alpha_v\beta_3$ is enriched in the l_d phase, characterized by a deficiency of NBD-DHPE, in excellent agreement with previous findings from our laboratory (29). Notably, this agreement between both data sets was obtained despite employing different anti-integrin antibodies (previous study: anti-$\alpha_v\beta_3$ Mab, clone LM609; current study: anti-β_3 MAb, clone HMb3-1), thus largely excluding experimental uncertainties in the E_{raft} analysis of integrins due to potential antibody-specific artifacts. CS-XY scans were also conducted on DOPC/DPPC/CHOL mixed bilayers of different CHOL content in the presence of VN [VN(+)]. Representative CS-XY scans (raw data) from these experiments are illustrated in Fig. 3, *G–L*. Specifically, confocal data of NBD-DHPE (Fig. 3, *G–I*) and Alexa 555 MAb-labeled integrin distributions

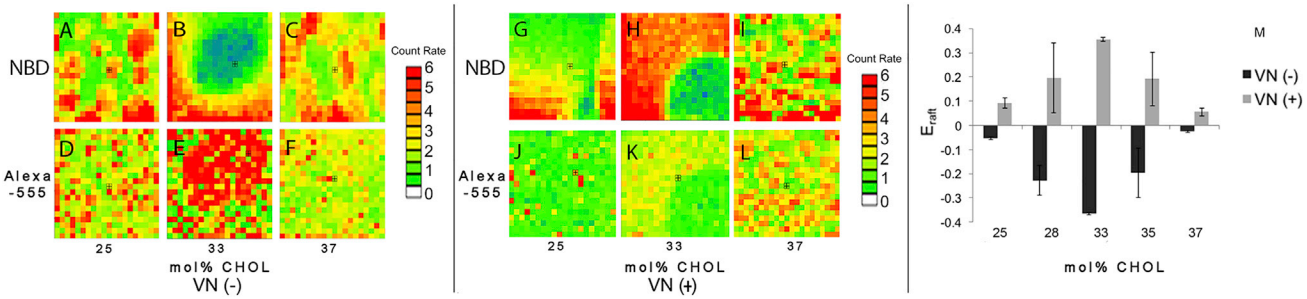

FIGURE 3 Representative CS-XY scans (raw data) of NBD-DHPE (*A–C* and *G–I*) and Alexa 555 MAb-tagged $\alpha_v\beta_3$-integrin distributions (*D–F* and *J–L*) in DOPC/DPPC/CHOL mixtures containing equimolar amounts of DOPC and DPPC and varying CHOL molar concentrations of 25, 33, and 37 mol%, as obtained through the NBD and Alexa 555 channels of the confocal detection system ($p < 0.01$). Separate data sets are presented for $\alpha_v\beta_3$ (*A–F*) and $\alpha_v\beta_3$ + VN (*G–L*). Quantification of the CS-XY data in terms of the parameter E_{raft} (see Eq. 1) demonstrates the profound influence of CHOL on the sequestration of $\alpha_v\beta_3$ before and after VN addition (*M*); $p < 0.01$ (box size; CS-XY scan: $12 \times 12\ \mu m^2$, pixel size: 0.5 μm). Error bars in (*M*) represent SD of E_{raft} acquisitions from 15 different bilayer regions (out of three samples). To see this figure in color, go online.

(Fig. 3, *J–L*) are presented for DOPC/DPPC/CHOL mixtures containing 25 (Fig. 3, *G* and *J*), 33 (Fig. 3, *H* and *K*), and 37 mol% CHOL (Fig. 3, *I* and *L*). Again, comparison of NBD and Alexa 555 channel data in Fig. 3, *G–K* demonstrates a lack of integrin sequestration for 25 (Fig. 3, *G* and *J*) and 37 mol% CHOL (Fig. 3, *I* and *L*), whereas $\alpha_V\beta_3$ sequestration consistent with the l_o-l_d phase boundaries can be observed in the case of 33 mol% CHOL (Fig. 3, *H* and *K*). In the latter case, however, regions of NBD-DHPE and Alexa 555 MAb-labeled $\alpha_v\beta_3$ with VN enrichments coincide, indicating l_o phase preference of $\alpha_v\beta_3$ upon VN binding. These findings are in very good agreement with earlier results in comparable membrane systems containing a 1:1:1 DOPC/DPPC/CHOL lipid mixture, which show that VN addition causes the net translocation of $\alpha_v\beta_3$ from l_d to l_o (29).

To obtain more quantitative information about the impact of CHOL on integrin sequestration in the absence and presence of VN, we next analyzed the background-corrected average signal intensities of the fluorescently tagged membrane proteins in the l_o and l_d phases from CS-XY scans using the parameter E_{raft} defined by Eq. 1. The bar graph in Fig. 3 *M* summarizes the resulting E_{raft} data of $\alpha_V\beta_3$ [VN(−)] (*light gray bars*) and $\alpha_V\beta_3$ with VN [VN(+)] (*dark gray bars*) in DOPC/DPPC/CHOL mixed bilayers containing 25, 28, 33, 35, and 37 mol% CHOL. Most notably, in both cases [VN(−) and VN(+)], there is a remarkable influence of CHOL content on integrin sequestration. In the absence of VN [VN(−)], the E_{raft} value for 25 mol% is slightly negative, but close to zero, indicating the lack of a particular l_o or l_d phase preference. Further increase in CHOL concentration to 28 and eventually 33 mol % is associated with gradually decreasing E_{raft} values, suggesting increasing l_d phase affinity. This l_d phase affinity gradually weakens again as the CHOL molar concentration is further increased to 35 and 37 mol% CHOL, thereby displaying no notable phase preference in the latter case. Intriguingly, the E_{raft} data for VN(+) show a remarkably similar pattern of CHOL dependence on integrin sequestration, albeit their positive values suggest an overall l_o phase affinity. Similar to the ligand-free case, the $\alpha_V\beta_3$ distribution in the presence of VN [VN(+)] lacks a particular phase preference at 25 and 37 mol% CHOL, shows intermediate degrees of sequestration at 28 and 35 mol% CHOL, and exhibits maximal sequestration at 33 mol% CHOL.

Changes in CHOL level do not alter integrin oligomerization state

Previous experiments at the cellular level have revealed a tantalizing relationship between the clustering of integrins in CHOL-enriched focal adhesions and the CHOL level in the plasma membrane (19,43). However, the underlying mechanisms of such a CHOL-mediated regulation of integrin distribution remain elusive. Therefore, to test the significance of a direct relationship between integrin clustering and CHOL level in a model membrane environment, we next determined the oligomerization state of $\alpha_V\beta_3$ in the absence and presence of VN [VN(−) and VN(+)] in DOPC/DPPC/CHOL mixtures of 25, 28, 33, 35, and 37 mol% CHOL using PCH analysis following procedures described previously (28,29). Fig. 4 summarizes the results from these experiments. Specifically, the representative domain-specific time scans of confocal fluorescence intensity (Fig. 4 *A*) and corresponding PCH curves (Fig. 4 *B*) of Alexa 555 MAb-labeled $\alpha_V\beta_3$ in a polymer-tethered lipid DOPC/DPPC/CHOL mixed bilayer containing 33 mol% CHOL reveal a similarity of l_o- and l_d-specific data. More importantly, the presented X_{dimer} data in Fig. 4 *C* demonstrate that systematic variations of CHOL molar concentration in the different lipid mixtures do not lead to statistically significant changes of $\alpha_V\beta_3$ oligomerization state regardless of the absence or presence of native ligands. In all lipid compositions investigated, Alexa 555-tagged $\alpha_v\beta_3$ display predominantly monomeric behavior, in good agreement with previous findings on full-length integrins in cellular studies (44). Taken together, comparison of E_{raft} and X_{dimer} data in Figs. 3 and 4, respectively, establishes that there is no

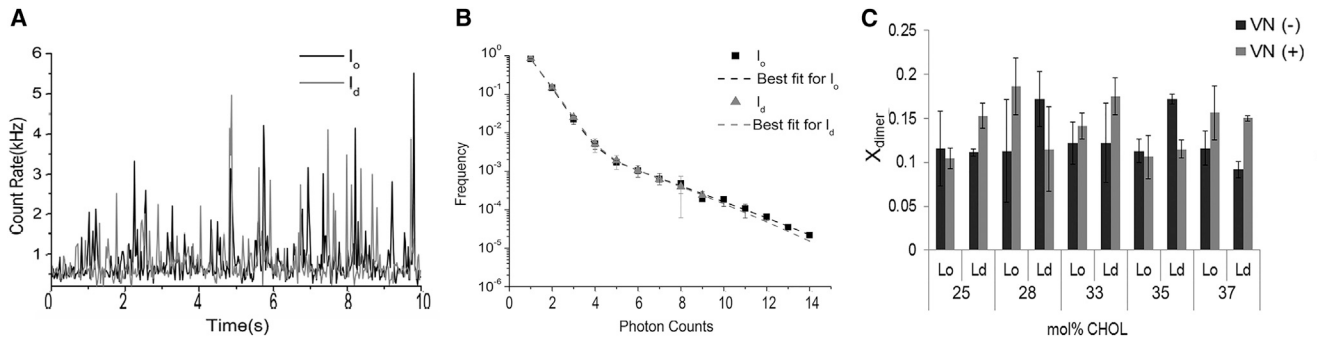

FIGURE 4 Representative time scans of confocal fluorescence intensity (*A*) and corresponding PCH curves (*B*) of Alexa 555 MAb-labeled $\alpha_v\beta_3$ in l_o and l_d domains in a polymer-tethered lipid bilayer comprised of an equimolar ratio of DOPC and DPPC and 33 mol% CHOL. Parameter X_{dimer} from PCH analysis demonstrates that changes in CHOL content do not alter the predominantly monomeric nature of integrins in the bilayer (*C*) ($p < 0.01$). Data in (*B*) and (*C*) are based on 50 independent data sets for each lipid composition. Errors bars represent standard deviation.

obvious correlation between the impact of CHOL level on integrin sequestration and the degree of integrin dimerization.

Integrin sequestration is more susceptible to alteration of CHOL level than sequestration of GPI-anchored uPAR

The substantial effect of CHOL level on integrin sequestration in Fig. 3 is remarkable if compared to the weaker influence of CHOL content on the sequestration of GPI-anchored uPAR in comparable lipid mixtures reported previously (28). As illustrated in Fig. 5, the differing impacts of CHOL level on the sequestration of $\alpha_V\beta_3$ and uPAR in ternary DOPC/DPPC/CHOL mixtures can be expressed in terms of the fraction of membrane proteins, expressed by the parameter $X_{migrate}$ (see Eq. 2), which translocate from one type of domain to the other in response to changes in CHOL molar concentration in the bilayer. Fig. 5 shows that variation of CHOL molar concentration from 33 to 37 mol% causes ~19% of integrins to alter their phase preference in a lipid bilayer of coexisting l_o and l_d domains. In contrast, only ~7% of uPAR proteins were found to translocate to another phase in response to a comparable change in CHOL level in the bilayer. These results are notable because they suggest that transmembrane proteins may be more susceptible to changes in CHOL level than GPI-anchored proteins. At first sight, this result is surprising if one follows earlier arguments that transmembrane proteins typically stay outside of lipid rafts, unless they are activated by specific ligands (45), whereas the lipid anchor of GPI-anchored proteins acts as a determining molecular motif for the raft affinity of these membrane proteins (46). The data in Fig. 5 become more plausible, however, if one also considers the potential importance of hydrophobic matching in l_o-l_d sequestration of transmembrane proteins. In contrast, comparable hydrophobic matching arguments cannot be made in the case of GPI-anchored proteins like uPAR (26,28), making the sequestration of these membrane proteins less susceptible to CHOL-mediated changes in bilayer thickness.

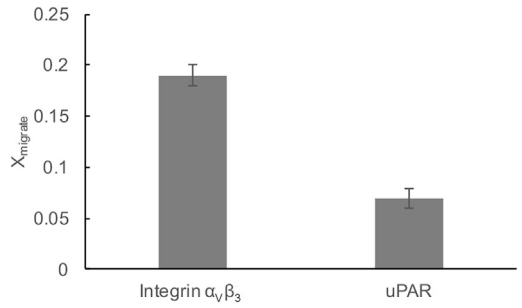

FIGURE 5 Populations of $\alpha_v\beta_3$ and uPAR, $X_{migrate}$ (defined by Eq. 2), in a polymer-tethered lipid bilayer, which alter their phase preference in a ternary DOPC/DPPC/CHOL mixture in response to a change in membrane CHOL from 33 to 37 mol%; $p < 0.005$. Data are based on 15 independent data sets of E_{raft} at 33 and 37 mol% CHOL. Errors bars represent corresponding standard deviation.

Potential mechanisms of CHOL-mediated integrin sequestration and implications for cellular studies

Comparison of domain-specific diffusion and sequestration data of dye-labeled lipids in Fig. 2, *A* and *B* with E_{raft} data of integrin distribution in Fig. 3 *M* shows a close correlation between the degree of l_d phase preference of integrins without ligands [VN(−)] and the extent of lipid packing difference between l_o and l_d phases. This interesting finding indicates the potential significance of domain-specific lipid packing as an important biophysical regulator of integrin sequestration. Indeed, such a biophysical mechanism agrees well with the recent analysis of energetic feasibility of CHOL-induced protein sorting, which emphasizes the important role of the energy penalty for incorporating membrane-spanning proteins into CHOL-enriched lipid domains (14). Hydrophobic matching arguments seem to be less significant in this case because structural data suggest a good hydrophobic match between the thickness of the transmembrane helices of the integrin α- and β-subunits of 31.6 ± 3.4 Å and 30.0 ± 3.6 Å (47,48) and the hydrophobic thickness of the l_d phase of 33 ± 1 Å. In contrast, a mechanism of CHOL-mediated regulation of integrin sequestration, due to lipid packing differences between l_o and l_d phases, is not plausible to explain the observed net translocation of integrins upon VN binding from the phase of lower lipid packing (l_d) to the phase of higher lipid packing (l_o). In this case, available integrin and bilayer structural data show a substantial mismatch between the hydrophobic transmembrane region thickness of integrins (47,48) and the thickness of the l_o bilayer region of 38 ± 1 Å (49), suggesting hydrophobic mismatch as a more dominant biophysical mechanism of membrane protein sequestration. Interestingly, the potential significance of hydrophobic matching was recently also demonstrated by determining that not only the lipid bilayer, but also incorporated membrane proteins (rhodopsin) adjust their structure to overcome hydrophobic mismatch (50). The substantial increase of transmembrane region thickness of integrins upon VN addition can be attributed to ligand-induced allosteric changes within the integrin receptor, which also influence its transmembrane region (25). For example, previous multiscale simulations on integrin α_{IIb}/β_3 confirmed that α_{IIb} mutations, which were found to have a significant effect on integrin activation (51), lead to a perturbation of transmembrane helix packing and changing crossing angles of the two integrin transmembrane helices from 35° (wild type) to 10° (mutation) (52). Taken together, our model membrane results suggest that the CHOL-mediated regulation of integrin sequestration can be attributed to biophysical mechanisms, which are associated with the

impact of CHOL on lipid packing and bilayer thickness. However, it remains challenging to deconvolute the individual contributions of lipid packing and hydrophobic matching in such a process.

Our experimental results are intriguing in light of the reported link between membrane CHOL and integrin signaling and adhesion (17,43). For example, it was previously determined that the formation of focal adhesions, which are highly enriched in CHOL (19), requires the controlled transport of CHOL to the plasma membrane, illustrating the potential significance of membrane CHOL adjustments in the regulation of protein functionality in cellular membranes (18). Interestingly, cellular focal adhesions represent sophisticated force sensors of remarkable dynamics and plasticity, which change their size in response to environmental stimuli during cell spreading and migration, thereby requiring the diffusive transport of integrins into and out of focal adhesion regions (53). Indeed, recent single-molecule fluorescence microscopy experiments demonstrated that focal adhesion regions largely consist of fluid membrane regions, dotted with small islands of clustered focal adhesion proteins (54), consistent with high resolution cryoelectron microscopy data of focal adhesion structure (55). The current model membrane study suggests that variations in membrane CHOL may have a notable impact on the distribution of integrins in a heterogeneous membrane environment. Here native integrin ligands could serve as regulators of integrin transport. In contrast to previous fluorescence resonance energy transfer-based experiments on S2 cells, which indicate a direct relationship between CHOL level and the degree of $\alpha_{PS2C}\beta_{PS}$ microclustering (56), our experiments suggest that changes in the model lipid composition per se (i.e., variations in CHOL concentration) are insufficient to modify the clustering state of integrins. Instead, our results support a concept in which the regulation of integrin clustering should be attributed to other factors, such as the presence of Mn^{2+} and the binding of certain adaptor proteins like talin (57).

CONCLUSIONS

This work demonstrates that changes in CHOL molar concentration have a significant influence on the sequestration of $\alpha_V\beta_3$ integrin in ternary DOPC/DPPC/CHOL mixtures forming coexisting l_o and l_d domains. This CHOL-dependence of integrin sequestration occurs regardless of the absence or presence of the native $\alpha_V\beta_3$ ligand VN. Although $\alpha_V\beta_3$ shows an overall affinity for the l_d phase in the ligand-free case, a switch to l_o phase preference can be observed upon VN addition without altering integrin oligomerization state. Notably, the presented model membrane data support a crucial role of CHOL in the assembly of integrin-based signal complexes and the assembly of integrin clusters at focal adhesions. Our experimental findings are significant because they suggest that the transport of integrins to/from CHOL-enriched membrane regions is, at least in part, regulated by a CHOL-dependent biophysical mechanism that does not alter the integrin oligomerization state. Due to the biophysical nature of this process, we anticipate that our current experimental findings also have implications for other membrane proteins. We hypothesize that a similar experimental approach will be suitable to explore the poorly understood role of lipid composition, such as CHOL content, on the assembly of signaling complexes of membrane proteins. Such model membrane experiments would benefit from the fact that protein processes can be monitored in heterogeneous lipid mixtures of well-defined compositions without the need for artificial cross-linking agents, a common challenge in cell experiments.

AUTHOR CONTRIBUTIONS

Y.G. and J.G. performed research. R.J. provided lipopolymers. C.A.N. designed research and wrote the manuscript.

ACKNOWLEDGMENTS

We thank Wolfgang Goldmann for helpful discussions.

This work was supported in part by the National Science Foundation (grant MCB-0920134) and the Indiana University-Purdue University Indianapolis Nanoscale Imaging Center.

REFERENCES

1. Simons, K., and R. Ehehalt. 2002. Cholesterol, lipid rafts, and disease. *J. Clin. Invest.* 110:597–603.
2. Burger, K., G. Gimpl, and F. Fahrenholz. 2000. Regulation of receptor function by cholesterol. *Cell. Mol. Life Sci.* 57:1577–1592.
3. Song, Y., A. K. Kenworthy, and C. R. Sanders. 2014. Cholesterol as a co-solvent and a ligand for membrane proteins. *Protein Sci.* 23:1–22.
4. Barrantes, F. J. 2004. Structural basis for lipid modulation of nicotinic acetylcholine receptor function. *Brain Res. Brain Res. Rev.* 47:71–95.
5. Pucadyil, T. J., and A. Chattopadhyay. 2006. Role of cholesterol in the function and organization of G-protein coupled receptors. *Prog. Lipid Res.* 45:295–333.
6. Brannigan, G., J. Hénin, …, M. L. Klein. 2008. Embedded cholesterol in the nicotinic acetylcholine receptor. *Proc. Natl. Acad. Sci. USA.* 105:14418–14423.
7. Crane, J. M., and L. K. Tamm. 2004. Role of cholesterol in the formation and nature of lipid rafts in planar and spherical model membranes. *Biophys. J.* 86:2965–2979.
8. Scherfeld, D., N. Kahya, and P. Schwille. 2003. Lipid dynamics and domain formation in model membranes composed of ternary mixtures of unsaturated and saturated phosphatidylcholines and cholesterol. *Biophys. J.* 85:3758–3768.
9. Kucerka, N., J. Pencer, …, J. Katsaras. 2007. Influence of cholesterol on the bilayer properties of monounsaturated phosphatidylcholine unilamellar vesicles. *Eur. Phys. J. E Soft Matter.* 23:247–254.
10. Bretscher, M. S., and S. Munro. 1993. Cholesterol and the golgi apparatus. *Science.* 261:1280–1281.
11. Kaiser, H. J., A. Orłowski, …, K. Simons. 2011. Lateral sorting in model membranes by cholesterol-mediated hydrophobic matching. *Proc. Natl. Acad. Sci. USA.* 108:16628–16633.
12. Brown, D. A., and E. London. 1998. Functions of lipid rafts in biological membranes. *Annu. Rev. Cell Dev. Biol.* 14:111–136.

13. Simons, K., and E. Ikonen. 1997. Functional rafts in cell membranes. *Nature.* 387:569–572.
14. Lundbaek, J. A., O. S. Andersen, …, C. Nielsen. 2003. Cholesterol-induced protein sorting: an analysis of energetic feasibility. *Biophys. J.* 84:2080–2089.
15. Schäfer, L. V., D. H. de Jong, …, S. J. Marrink. 2011. Lipid packing drives the segregation of transmembrane helices into disordered lipid domains in model membranes. *Proc. Natl. Acad. Sci. USA.* 108:1343–1348.
16. Milovanovic, D., A. Honigmann, …, R. Jahn. 2015. Hydrophobic mismatch sorts SNARE proteins into distinct membrane domains. *Nat. Commun.* 6:5984.
17. Green, J. M., A. Zheleznyak, …, E. J. Brown. 1999. Role of cholesterol in formation and function of a signaling complex involving alphavbeta3, integrin-associated protein (CD47), and heterotrimeric G proteins. *J. Cell Biol.* 146:673–682.
18. del Pozo, M. A., N. B. Alderson, …, M. A. Schwartz. 2004. Integrins regulate Rac targeting by internalization of membrane domains. *Science.* 303:839–842.
19. Gaus, K., S. Le Lay, …, M. A. Schwartz. 2006. Integrin-mediated adhesion regulates membrane order. *J. Cell Biol.* 174:725–734.
20. Leitinger, B., and N. Hogg. 2002. The involvement of lipid rafts in the regulation of integrin function. *J. Cell Sci.* 115:963–972.
21. Kalli, A. C., T. Rog, …, M. S. Sansom. 2016. The integrin receptor in biologically relevant bilayers: insights from molecular dynamics simulations. *J. Membr. Biol.* 250:337–351.
22. Hancock, J. F. 2006. Lipid rafts: contentious only from simplistic standpoints. *Nat. Rev. Mol. Cell Biol.* 7:456–462.
23. Lingwood, D., and K. Simons. 2010. Lipid rafts as a membrane-organizing principle. *Science.* 327:46–50.
24. Kahya, N., D. A. Brown, and P. Schwille. 2005. Raft partitioning and dynamic behavior of human placental alkaline phosphatase in giant unilamellar vesicles. *Biochemistry.* 44:7479–7489.
25. Baumgart, T., A. T. Hammond, …, W. W. Webb. 2007. Large-scale fluid/fluid phase separation of proteins and lipids in giant plasma membrane vesicles. *Proc. Natl. Acad. Sci. USA.* 104:3165–3170.
26. Cunningham, O., A. Andolfo, …, N. Sidenius. 2003. Dimerization controls the lipid raft partitioning of uPAR/CD87 and regulates its biological functions. *EMBO J.* 22:5994–6003.
27. Caiolfa, V. R., M. Zamai, …, N. Sidenius. 2007. Monomer dimer dynamics and distribution of GPI-anchored uPAR are determined by cell surface protein assemblies. *J. Cell Biol.* 179:1067–1082.
28. Ge, Y., A. P. Siegel, …, C. A. Naumann. 2014. Ligand binding alters dimerization and sequestering of urokinase receptors in raft-mimicking lipid mixtures. *Biophys. J.* 107:2101–2111.
29. Siegel, A. P., A. Kimble-Hill, …, C. A. Naumann. 2011. Native ligands change integrin sequestering but not oligomerization in raft-mimicking lipid mixtures. *Biophys. J.* 101:1642–1650.
30. Hussain, N. F., A. P. Siegel, …, C. A. Naumann. 2013. Bilayer asymmetry influences integrin sequestering in raft-mimicking lipid mixtures. *Biophys. J.* 104:2212–2221.
31. Lüdtke, K., R. Jordan, …, C. A. Naumann. 2005. Lipopolymers from new 2-substituted-2-oxazolines for artificial cell membrane constructs. *Macromol. Biosci.* 5:384–393.
32. Garg, S., J. Rühe, …, C. A. Naumann. 2007. Domain registration in raft-mimicking lipid mixtures studied using polymer-tethered lipid bilayers. *Biophys. J.* 92:1263–1270.
33. Deverall, M. A., E. Gindl, …, C. A. Naumann. 2005. Membrane lateral mobility obstructed by polymer-tethered lipids studied at the single molecule level. *Biophys. J.* 88:1875–1886.
34. Rigaud, J.-L., and D. Lévy. 2003. Reconstitution of membrane proteins into liposomes. *Methods Enzymol.* 372:65–86.
35. Byron, A., J. D. Humphries, …, M. J. Humphries. 2009. Anti-integrin monoclonal antibodies. *J. Cell Sci.* 122:4009–4011.
36. Carman, C. V. 2012. Overview: imaging in the study of integrins. *Methods Mol. Biol.* 757:159–189.
37. Murcia, M. J., D. E. Minner, …, C. A. Naumann. 2008. Design of quantum dot-conjugated lipids for long-term, high-speed tracking experiments on cell surfaces. *J. Am. Chem. Soc.* 130:15054–15062.
38. Veatch, S. L., and S. L. Keller. 2003. Separation of liquid phases in giant vesicles of ternary mixtures of phospholipids and cholesterol. *Biophys. J.* 85:3074–3083.
39. Kiessling, V., J. M. Crane, and L. K. Tamm. 2006. Transbilayer effects of raft-like lipid domains in asymmetric planar bilayers measured by single molecule tracking. *Biophys. J.* 91:3313–3326.
40. Veatch, S. L., O. Soubias, …, K. Gawrisch. 2007. Critical fluctuations in domain-forming lipid mixtures. *Proc. Natl. Acad. Sci. USA.* 104:17650–17655.
41. Ke, P. C., and C. A. Naumann. 2001. Hindered diffusion in polymer-tethered phospholipid monolayers at the air-water interface: a single molecule fluorescence imaging study. *Langmuir.* 17:5076–5081.
42. Sezgin, E., I. Levental, …, P. Schwille. 2012. Partitioning, diffusion, and ligand binding of raft lipid analogs in model and cellular plasma membranes. *Biochim. Biophys. Acta.* 1818:1777–1784.
43. Norambuena, A., and M. A. Schwartz. 2011. Effects of integrin-mediated cell adhesion on plasma membrane lipid raft components and signaling. *Mol. Biol. Cell.* 22:3456–3464.
44. Wang, W., J. Zhu, …, B. H. Luo. 2011. Tests of integrin transmembrane domain homo-oligomerization during integrin ligand binding and signaling. *J. Biol. Chem.* 286:1860–1867.
45. Cherukuri, A., M. Dykstra, and S. K. Pierce. 2001. Floating the raft hypothesis: lipid rafts play a role in immune cell activation. *Immunity.* 14:657–660.
46. Brown, D. A., and J. K. Rose. 1992. Sorting of GPI-anchored proteins to glycolipid-enriched membrane subdomains during transport to the apical cell surface. *Cell.* 68:533–544.
47. Lomize, A., M. lomize, and I. Pogozheva. 2005–2011. Membranome database -human membrane atlas (Integrin alpha-V).. College of Pharmacy, University of Michigan, Ann Arbor, MI.
48. Lomize, A., M. lomize, and I. Pogozheva. 2005–2011. Orientations of proteins in membranes (OPM) database (Integrin beta-3, transmembrane helix).. Mosberg Laboratory, College of Pharmacy, University of Michigan, Ann Arbor, MI.
49. Gandhavadi, M., D. Allende, …, T. J. McIntosh. 2002. Structure, composition, and peptide binding properties of detergent soluble bilayers and detergent resistant rafts. *Biophys. J.* 82:1469–1482.
50. Soubias, O., W. E. Teague, Jr., …, K. Gawrisch. 2015. Rhodopsin/lipid hydrophobic matching-rhodopsin oligomerization and function. *Biophys. J.* 108:1125–1132.
51. Hughes, P. E., F. Diaz-Gonzalez, …, M. H. Ginsberg. 1996. Breaking the integrin hinge. A defined structural constraint regulates integrin signaling. *J. Biol. Chem.* 271:6571–6574.
52. Kalli, A. C., I. D. Campbell, and M. S. P. Sansom. 2011. Multiscale simulations suggest a mechanism for integrin inside-out activation. *Proc. Natl. Acad. Sci. USA.* 108:11890–11895.
53. Geiger, B., J. P. Spatz, and A. D. Bershadsky. 2009. Environmental sensing through focal adhesions. *Nat. Rev. Mol. Cell Biol.* 10:21–33.
54. Shibata, A. C., L. H. Chen, …, A. Kusumi. 2013. Rac1 recruitment to the archipelago structure of the focal adhesion through the fluid membrane as revealed by single-molecule analysis. *Cytoskeleton (Hoboken).* 70:161–177.
55. Patla, I., T. Volberg, …, O. Medalia. 2010. Dissecting the molecular architecture of integrin adhesion sites by cryo-electron tomography. *Nat. Cell Biol.* 12:909–915.
56. Dibya, D., N. Arora, and E. A. Smith. 2010. Noninvasive measurements of integrin microclustering under altered membrane cholesterol levels. *Biophys. J.* 99:853–861.
57. Cluzel, C., F. Saltel, …, B. Wehrle-Haller. 2005. The mechanisms and dynamics of (alpha)v(beta)3 integrin clustering in living cells. *J. Cell Biol.* 171:383–392.